



Iron phosphides presenting different stoichiometry as nanocatalysts in the HDO of phenol

E. Rodríguez-Aguado^a, A. Infantes-Molina^{a,*}, D. Ballesteros-Plata^a, J.F. Marco^b, E. Moretti^c, E. Finocchio^d, J.A. Cecilia^a, E. Rodríguez-Castellón^{a,*}

^a Departamento de Química Inorgánica, Cristalografía y Mineralogía (Unidad Asociada al ICP-CSIC), Facultad de Ciencias, Universidad de Málaga, Campus de Teatinos, 29071 Málaga, Spain

^b Instituto de Química Física Rocasolano, CSIC, Madrid, Spain

^c Dipartimento di Scienze Molecolari e Nanosistemi, Università Ca' Foscari Venezia, INSTM Venice Research Unit, Mestre Venezia, Italy

^d Dipartimento di Ingegneria Civile, Chimica e Ambientale, Università degli Studi di Genova, Génova, Italy

ARTICLE INFO

Keywords:

Iron phosphide
HDO
Heterogeneous catalysis
Silica
Phenol

ABSTRACT

Iron phosphide catalysts supported on silica with an iron loading of 15 wt% were synthesized and studied in the hydrodeoxygenation (HDO) of phenol. The amount of phosphorus varied in order to obtain iron phosphides with different stoichiometry. Catalysts containing Fe₂P, FeP and FeP₂ phases were obtained. The textural and structural properties of the prepared catalysts were evaluated by using different experimental techniques such as N₂ adsorption-desorption at -196 °C, X-ray diffraction (XRD), Mössbauer spectroscopy, high resolution transmission spectroscopy (HRTEM), infrared spectroscopy (IR) of adsorbed CO at low temperature, X-ray photoelectron microscopy (XPS) and NH₃ thermoprogrammed desorption (NH₃-TPD). The catalytic activity was studied at 275 °C and at 15 and 5 bar of hydrogen pressure in the hydrodeoxygenation reaction of phenol. Characterization results evidenced that the initial P/Fe ratio employed in the synthesis not only governed the stoichiometry of the iron phosphide, but also the particle size, metallic surface exposure and acidity. The catalysts presenting unique phases were those presenting better activity in the HDO reaction of phenol. Moreover, Fe₂P phase presented better results than FeP in terms of HDO conversion.

1. Introduction

Increasingly awareness on polluted atmospheric environment combined with depletion of fossil fuels and increased reliance on unconventional crude oil resources which need to be highly purified, are prompting many researchers to address this problematic. Thus, new approaches on hydrotreating processes are being tackled as well as the search of new catalytic materials for processing fossil fuel feedstocks [1]. In this sense, fast pyrolysis of solid lignocellulosic biomass has drawn considerable attention for the production of liquid biofuels as this type of biomass is renewable and easily available [2–4]. Indeed, this process can be efficiently applied to commercial plants without investing a high amount of capital. However, the obtained bio-oil must be upgraded to ensure the removal of a wide variety of oxygenated compounds. The removal of oxygen can be tackled by means of hydrodeoxygenation, which is regarded as an effective method to improve the effective H/C ratio [5,6]. During HDO, oxygenated compounds are converted to hydrocarbons under hydrogen pressure and in the presence of heterogeneous catalysts. Currently, HDO faces several

challenges, which have to be solved to expand its use in the already existing biorefineries [7,8]. In this respect, the consumption of low levels of hydrogen along with the obtainment of a high degree of deoxygenation is one of the most important challenges. Therefore, the catalyst design is a key factor to cope with that purpose. Typically, catalysts used in the HDO reactions are constituted by a metal with good hydrogen transfer properties supported on a high surface area oxide support. Conventional sulfide catalysts such as CoMoS and NiMoS, used in petroleum hydrodesulfurization, have been used in HDO reactions; however, the oxidation of the sulfide species by the presence of H₂O, obtained as by-product in the HDO reaction, and the formation of carbonaceous deposits cause a strong deactivation of the active phase [9,10]. Catalysts based on noble metals have also been widely studied but their high activity does not offset their high cost. That is why alternative catalysts as those constituted by transition metal phosphides have attracted great attention in recent years since they have much lower costs and their electronic structure is close to that of noble metals [11,12]. Concretely, transition metal phosphides have resulted to be very active in hydrotreating reactions also showing high

* Corresponding authors.

E-mail addresses: ainfantes@uma.es (A. Infantes-Molina), castellon@uma.es (E. Rodríguez-Castellón).

<https://doi.org/10.1016/j.cattod.2018.05.023>

Received 17 December 2017; Received in revised form 5 May 2018; Accepted 10 May 2018
0920-5861/ © 2018 Elsevier B.V. All rights reserved.

stability and resistance to deactivation in the presence of water. Several studies of the HDO of diluted oxygenated compound solutions with transition metal phosphides have been reported, having shown remarkable results in terms of activity, stability and durability [12–16]. Most of the studies have proved that nickel phosphide based catalysts display the most suitable properties to carry out an excellent performance on the HDO process [17–19]. However, although it is necessary to search highly active catalysts it is also essential to employ cheaper, abundant and non-toxic active phases, which is another challenge that HDO must face to be implemented industrially. In that sense, the present research has synthesized a series of phosphides containing iron as active phase to cope with that challenge.

The use of iron phosphide in the hydrotreating field has been scarce. It has been reported in the literature that Oyama et al. [12–14] carried out preliminary analysis in hydrodesulfurization (HDS), hydrodenitrogenation (HDN) and hydrodeoxygenation (HDO) reactions for target molecules coming from the petrochemical industry and lignocellulosic biomass. More recently, Huang et al. [20] have also studied the catalytic activity of iron phosphide based catalysts in the HDS of thiophene; while Yuan et al. [21] have evaluated the catalytic behavior of FeP and FeP₂ in the HDS of dibenzothiophene, HDN of quinoline and hydrogenation of tetralin to decalin, obtaining the highest conversions for the FeP based catalysts. Currently, iron phosphide based catalysts are highly studied as efficient electrocatalyst and photocatalyst for the oxygen and hydrogen evolution reactions [22–25]. The use of iron as promoter of nickel phosphide based catalysts has also been evaluated since the incorporation of iron can alter the electronic density of the active phase, modifying the selectivity pattern [26–28].

In summary, although there are some reports concerning the catalytic behavior of iron based phosphides, none of them have focused on the effects of the stoichiometry of the iron phosphide based catalysts in HDO reactions. In previous works, it has been reported that phosphides based on Ni and Co prepared from phosphite-type precursors displayed a good catalytic performance in the HDO of phenol [18]. In addition, the effect of the initial P/Metal ratio on their catalytic response was studied, having proved that the stoichiometry of the phosphide formed has direct effects on the catalytic process [15,29]. It is also known that the effect of phosphorus strongly depends on its content, showing a negative effect at high loadings. In the present work, the characterization and catalytic activity of iron phosphide supported catalysts presenting different stoichiometry by changing the initial P/Fe ratio is reported. Thus, the possible application of a cheap and non-toxic phase such as iron in the form of iron phosphide is going to be evaluated. HDO of phenol, as an oxygenated model compound present on fast-pyrolysis bio-oil from lignocellulosic biomass, was the catalytic test chosen to evaluate the activity.

2. Materials and methods

2.1. Materials

The catalytic support used in this study was a commercial fumed silica from Sigma-Aldrich. The reagents used to prepare the precursor solution were iron(III) nitrate nonahydrate (Fe(NO₃)₃·9H₂O, 98%, Alfa Aesar) and phosphorous acid (H₂PO₃H, 99%, Analyticals). In the reactivity study, phenol (98%, Amresco) was used as oxygenated compound; octane (99%, Sigma-Aldrich) was used as solvent and nonane (99%, Sigma-Aldrich) as internal standard. The gases employed were He (Air Liquide 99.999%), H₂ (Air Liquide 99.999%), N₂ (Air Liquide 99.9999%), CO (Air Liquide 99.9%) and NH₃ (Air Liquide 99.99%).

2.2. Preparation of catalysts

Iron based catalysts (15 wt%) were prepared by incipient wetness impregnation of the silica support by adding different amounts of iron (III) nitrate nonahydrate and phosphorous acid (H₂PO₃H) to achieve P/

Fe molar ratios of 0.5, 1, 2 and 3 as described elsewhere [30], where it is described the preparation of phosphides by using hydrogenophosphite as a precursor salt. The impregnated supports were air-treated at 60 °C for 24 h and finally, the precursors were reduced ex-situ under a hydrogen flow of 100 mL min⁻¹ in a tubular reactor by heating from rt to 300 °C (over a temperature linear ramp of 10 °C min⁻¹ and from 300 to 700 °C (3 °C min⁻¹) remaining 2 h at that temperature. After reduction, the iron phosphides based catalysts were cooled to room temperature under He flow and then passivated under 100 mL min⁻¹ of 0.5% O₂/N₂ (Air Liquid) flow for 4 h at room temperature. The series of iron phosphides were prepared by maintaining constant the iron content (15 wt%) and varying the initial P/Fe molar ratio. Thus, the synthesized catalysts were denoted as P/Fe-x, where x is the P/Fe molar ratio employed, x = 0.5, 1, 2 and 3.

2.3. Characterization of catalysts

The textural parameters of the passivated catalysts were evaluated from N₂ adsorption-desorption isotherms at -196 °C measured using an automatic ASAP 2020 system (Micromeritics). Before measurements, samples were outgassed at 150 °C and 10⁻⁴ mbar overnight. Specific surface areas (S_{BET}) were determined by using the BET equation considering a N₂ cross section of 16.2 Å².

Metal Dispersion was calculated from CO-chemisorption measurements. CO uptakes were measured in a Micromeritics ASAP 2020 apparatus. Prior to measurement, the samples were re-reduced in situ in H₂ at 450 °C and then evacuated at 25 °C for 10 h. The chemisorption isotherm was obtained by measuring the amount of CO adsorbed between 10 and 600 mmHg at 35 °C. After completing the initial analysis, the reversibly adsorbed gas was evacuated and the analysis was repeated to determine only the chemisorbed amounts.

$$\text{Dispersion (\%)} = \frac{\text{CO uptake (mmoles/g)}}{\text{Metal loading (}\frac{\text{mmoles}}{\text{g}}\text{)}}$$

Powder diffraction patterns were collected using a X'Pert Pro MPD automated diffractometer (PANalytical) with Mo-K α radiation ($\lambda = 0.70930$ Å), scanning from 9 to 27° (2 θ). The crystallographic phases were identified by using Highscore Plus software from PANalytical.

Mössbauer data were recorded at room temperature in the transmission mode using a conventional constant acceleration spectrometer equipped with a ⁵⁷Co(Rh) source. An effective absorber thickness of 5 mg cm⁻² of natural iron was used for all the samples. The velocity scale was calibrated using a 6 μ m thick α -Fe foil. All the spectra were computer-fitted and the isomer shifts were referred to the centroid of the spectrum of α -Fe at room temperature.

Size and morphology of the catalysts were studied by high resolution transmission electron microscopy (HR-TEM) using a TALOS F200x instrument. TEM analysis was performed at 200 kV and 5.5 μ A and scanning transmission electron microscopy (STEM) with a HAADF detector, at 200 kV and 200 nA.

The Fourier transform infrared (FT-IR) spectra were carried out with a Nicolet Nexus instrument, using a conventional cell connected to a gas-handling system. Prior to each adsorption, pressed disks of powder samples with a diameter of 1.5 cm (ca. 20 mg) were thermally treated within the cell at 400 °C under H₂ (40 kPa) for 1 h. Then, the samples were outgassed at 400 °C and cooled to carry out the spectrum at rt between 4000 and 400 cm⁻¹ using 200 scans and a resolution of 2 cm⁻¹. CO adsorption (0.13 kPa) experiments were performed at -140 °C and the spectra were recorded in the range of -140 to 10 °C while degassing.

Temperature-programmed desorption of ammonia (NH₃-TPD) was conducted to determine the acidity of the samples. For the experiments, 80 mg of catalytic precursors were reduced in-situ by flowing hydrogen to 700 °C (same conditions as in 2.2 section). Subsequently, samples

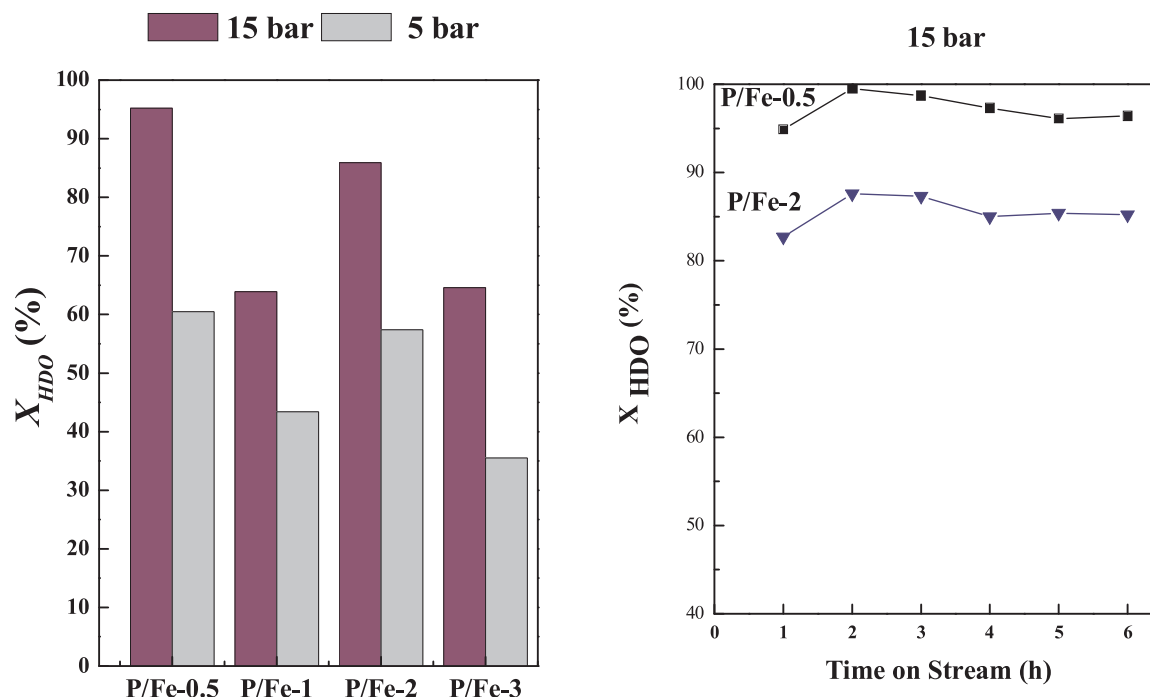


Fig. 1. A) HDO conversion for the different catalysts at ToS = 6 h and B) Evolution of the conversion with time on stream. Operating at 275 °C and WHSV = 0.4 h⁻¹.

were cooled to 100 °C and then exposed to flowing pure ammonia for 5 min. After ammonia adsorption, samples were cleaned with He flow in order to remove the physisorbed ammonia. Desorption was performed between 100 and 500 °C (10 °C·min⁻¹) and the desorbed ammonia was analyzed online by a thermal conductivity detector (TCD). In order to quantify the amount of ammonia desorbed, the equipment was previously calibrated by measuring the corresponding signals of the thermal decomposition of known amounts of hexaamminenickel(II) chloride, [Ni(NH₃)₆]Cl₂, supplied by Aldrich.

X-Ray Photoelectron spectroscopy (XPS) was conducted to study the surface composition of samples. Spectra were collected using a Physical Electronics PHI 5700 spectrometer with non-monochromatic Mg K α radiation (300 W, 15 kV, 1253.6 eV) with a multi-channel detector. Spectra of passivated samples were recorded in constant pass energy mode at 29.35 eV using a 720 μ m diameter analysis area. Binding energy (BE) values were referenced to the C 1s peak (284.8 eV) from the adventitious contamination layer. The PHI ACCESS ESCA-V6.0 F software package and Multipak v8.2b were used for acquisition and data analysis, respectively. A Shirley-type background was subtracted from the signals. Recorded spectra were fitted using Gauss-Lorentz curves, in order to determine the binding energy of the different element core levels more accurately. The error in BE was estimated to be ca. 0.1 eV.

2.4. Catalytic test

The hydrodeoxygenation of phenol was performed in a high-pressure, fixed-bed, continuous flow, stainless steel catalytic reactor (9.1 mm in diameter, 230 mm in length), operated in the down-flow mode. The reaction temperature was measured with an interior thermocouple in direct contact with the catalyst bed. The organic feed consisted on a solution of phenol (1 wt%) in octane which was supplied by means of a Gilson 307SC piston pump (model 10SC) with a flow rate of 0.18 ml·min⁻¹. For the activity test, 0.25 g of pelletized and passivated catalyst were transferred into the reaction tube diluted with carborundum to a total volume of 3 cm³ (particle size 0.85–1.18 mm). Prior to the activity test, samples were treated in-situ at atmospheric pressure with a H₂ flow of 100 mL·min⁻¹ by heating from rt to 450 °C (2 h) to ensure total reduction of the surface passivation layer. Catalytic

activities were measured at 275 °C under 5 and 15 bar, with a H₂ flow rate of 30 ml·min⁻¹ and weight hourly space velocity of 0.3 h⁻¹.

The evolution of the reaction was monitored by collecting liquid samples which were kept in sealed vials and subsequently analyzed by gas chromatography (Shimadzu GC-14B, equipped with a flame ionization detector and a capillary column, TBR-14, coupled to an automatic Shimadzu AOC-20i injector).

The HDO conversion was calculated by using the following equation:

$$\text{HDOConv. (\%)} = \frac{C_{\text{Ph. Ini}} - C_{\text{Ph. Fin}} - C_{\text{Int}}}{C_{\text{Ph. Ini}}} \times 100$$

where $C_{\text{Ph. Ini}}$ is the phenol concentration in the feed, $C_{\text{Ph. Fin}}$ is the phenol concentration in the liquid product and C_{Int} is the concentration of the O-containing intermediates.

Selectivity data were calculated considering all the reaction products by using the following equation:

$$S_i(\%) = \frac{C_i}{\sum_{i=1}^n C_i} \times 100$$

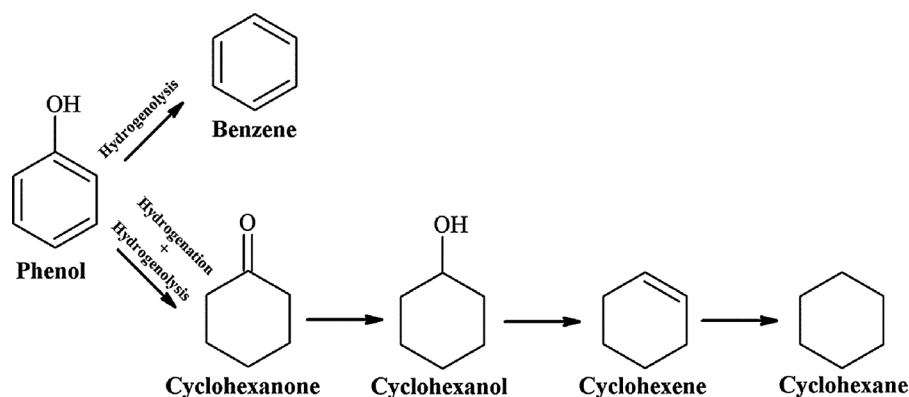
Where S_i is the selectivity of i-compound, C_i is the concentration of i-product and is the sum of concentration of all reaction products. The turnover frequency (TOF) was calculated from the formula:

$$\text{TOF} = \frac{F/W}{M} \times \ln(1 - X)$$

where F is the molar rate of the reaction (mol min⁻¹), W is the catalyst weight (g), X is the conversion factor and M is the number of sites loaded (mol g⁻¹). This formula was used because the conversion values were close to 100% and were far from differential conditions making an integral analysis necessary.

3. Results and discussion

The HDO reaction of phenol over the prepared materials was carried out at 275 °C and under pressures of 5 and 15 bar. The detailed reaction conditions are included in the experimental section. Fig. 1 represents a comparison of the HDO conversion values working under 5 and 15 bar.



The results reflect the strong dependency of the pressure on the activity of the catalysts being far superior working at higher pressure. Under 15 bar, all the catalysts result to be considerably active, achieving conversions values higher than 60% in all cases. At 15 bar, P/Fe-0.5 and P/Fe-2 samples are those more active. Working under 5 bar, the conversion values range from 40 to 60%. Again, P/Fe-0.5 and P/Fe-2 samples present better conversion values. Therefore, the evolution of HDO conversion at 15 bar of these catalysts versus time on stream is depicted in Fig. 1B. As observed in this graph, both catalysts present a growing catalytic response during the first two hours on stream, followed by a slight loss of catalytic activity which eventually remains steady during last two hours of time on stream.

Considering the selectivity results, it has been reported in literature that phenol hydrodeoxygenation can take place by direct hydrogenolysis of the C–O bond, obtaining benzene or by hydrogenation of the aromatic ring giving cyclohexanol and subsequent dehydration to obtain cyclohexene and later cyclohexane. As mentioned above, the catalytic results seem to indicate that the reaction proceeds via this second pathway, see Scheme 1, which is in agreement with previous research with nickel and cobalt phosphide based catalysts [28,29].

The selectivity results presented by iron phosphide based samples are included in Fig. 2. The selectivity values are strongly dependent on the reaction pressure studied. Thus, at 15 bar, the majority product is

cyclohexane, with selectivity values higher than 80%. Benzene and cyclohexene are also obtained but in much lesser extent. Instead, at 5 bar, the selectivity to cyclohexene increases conspicuously being the most important product in the case of P/Fe-3 sample. This suggests that all tested catalysts react via hydrogenation of the aromatic ring followed by dehydration of cyclohexanol to obtain cyclohexene and in a minority, benzene.

In the case of metallic phosphides, it has been suggested that coordinatively unsaturated metal sites (CUS) can act as Lewis sites, while surface oxygen behaves as Lewis basic sites [32]. Moreover, literature data report that phenol is adsorbed by a heterolytic dissociation between the hydrogen of its –OH group on the oxygen sites in the oxide surface layer leading to a phenoxide species [33] (Scheme 2), which are stabilized by the existence of coordinatively unsaturated metal sites (CUS) that act as Lewis sites [32]. Other authors have pointed out that phenol adsorption can also proceed by the existence of Lewis sites (Fe^{3+}) or the presence of defects in the grain boundary that are favored in small crystals by its interaction with the aromatic ring [34,35]. In the next step, the metallic species (Fe_xP_y) hydrogenates the aromatic ring to form cyclohexanone, being reduced to cyclohexanol easily. Finally, cyclohexanol –OH group interacts with the metal sites (Fe_xP_y) favoring its dehydration to cyclohexene and a subsequent hydrogenation to form cyclohexane [35].

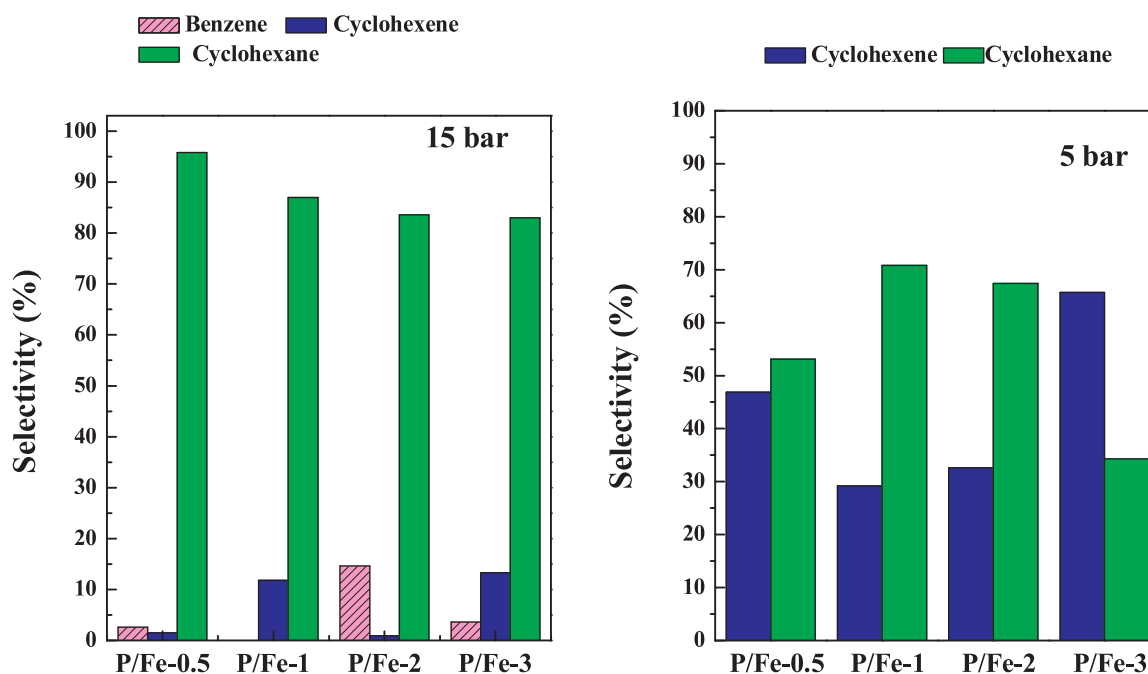
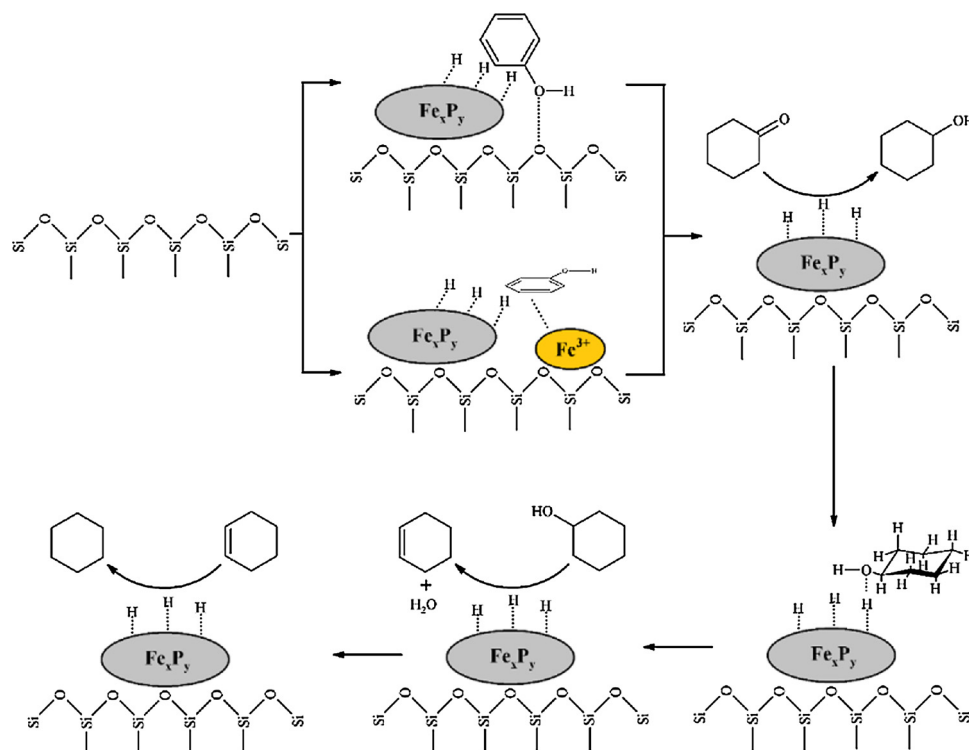


Fig. 2. Selectivity graphs for the studied catalysts under 5 and 15 bar, 275 °C, WHSV = 0.3 h⁻¹, ToS = 6 h.



Scheme 2. Proposed mechanism of Phenol HDO over Fe_xP_y samples.

Previous researchers have evaluated the catalytic behavior of iron catalysts supported on silica and carbon using guaiacol as target lignin molecule, at atmospheric pressure and high contact times [36,37]. These works reported the formation of phenol and benzene, discarding the hydrogenation of the aromatic ring. In the present research, the iron phosphide based catalysts were studied at higher H_2 pressure and lower contact time favoring the formation of dearomatized products (cyclohexene and cyclohexane). These data suggest that the hydrogenation of the aromatic ring is favored by the presence of H_2 -pressure, but also the iron phase plays an important role. Considering the functional groups of phenol, the $-\text{OH}$ group tends to interact with the active sites at milder reaction conditions, while the interaction of the aromatic ring with the metal sites is favored under more severe conditions. In this sense, it is well reported in the literature the hydrogenation of benzene to form cyclohexane under H_2 -pressure using Fe-based catalysts [38,39].

In order to understand and correlate the catalytic behavior of these catalysts with their properties a deep characterization was performed. The textural characterization as a result of N_2 adsorption-desorption analysis of the samples is included in Table 1. The textural properties of the bare support are also included for comparative purposes. Fig. 3 shows the corresponding isotherms (Fig. 3a) and pore size distribution graphs (Fig. 3b). The isotherms are all of type II and characteristic of solids with pores of diameters in the range of meso and macropores, and generally attributed to interparticle voids. BET surface areas suffer a remarkable decrease in comparison with the bare support as a

consequence of the incorporation of the active phases. As reported in previous works, this loss of specific surface area is attributed to the blockage of the surface pores with phosphorus species in excess [28,29]. Considering the pore size distribution, in all cases a bimodal distribution is observed compared to pure silica where not a clear pore size distribution is obtained. The sharp increase in the pore volume of the iron containing catalysts at high relative pressures suggests the formation of pores of bigger size in the range of macroporous such is our case. In this regard, all samples present a maximum close to 50 nm; however, pores of smaller size (22–27 nm) are also present and being much more important in the case of samples with an intermediate P/Fe molar ratio. In fact, P/Fe-1 is that presenting pores with smaller size and their proportion being as important as that of higher size.

The crystalline phases identified by XRD are shown in Fig. 4. The diffractograms were measured with monochromatic $\text{Mo K}\alpha$ radiation in order to diminish iron fluorescence. At first sight, the presence of different phosphide phases as a function of the initial P/Fe ratio is evident. Hence, P/Fe-0.5 catalyst presents diffraction peaks at 18.2, 19.9, 21.3, 23.7, 24.2 and 24.4° which are all assigned to the Fe_2P phase (PDF N°: 01-085-1725). By increasing the amount of P present in the catalyst formulation until P/Fe-1, the diffraction peaks ascribed to Fe_2P phase diminish and new ones appear at 14.1, 14.9, 15.7, 16.1, 16.9, 20.8, 21.1, 21.7, 22.6, 24.7 and 24.9°, which correspond to an iron phosphide phase richer in phosphorus such as FeP (PDF N°: 01-078-1443).

As the P content increases, Fe_2P phase disappears and for P/Fe-2 sample, FeP phase becomes the dominant and unique phase. By increasing the P/Fe ratio until 3, the catalyst with the greater content in phosphorus, besides the presence of the FeP phase, new diffraction lines emerge at 14.4, 16.6, 17.1, 17.9, 18.5, 21.9, 22.4, 23.2, 23.4, 25.8 and 26.4°. These reflection lines are ascribed to the presence of a new phase enriched in phosphorus, FeP_2 (PDF N°: 03-065-6088). So, from these data it can be concluded that in so far as the P content increases the formation of phosphorus richer phosphides takes place. Scherrer's equation was used to determine the average particle size of the various phases present and the corresponding data included in Table 2. From this table it can be observed that Fe_2P phase is more dispersed on P/Fe-

Table 1
Textural and acidic properties of the catalysts.

Sample	S_{BET} ($\text{m}^2 \text{g}^{-1}$)	V_p ($\text{cm}^3 \text{g}^{-1}$)	Total acidity (mmol NH_3/g)
SiO_2	203	0.64	–
P/Fe-0.5	82	0.77	0.06
P/Fe-1	100	0.62	0.09
P/Fe-2	76	0.64	0.22
P/Fe-3	61	0.56	0.15

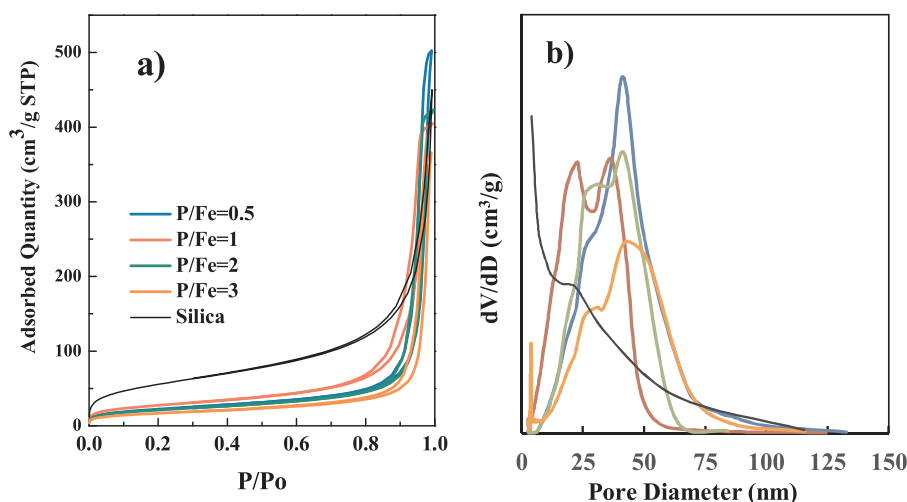


Fig. 3. N_2 -adsorption-desorption isotherms (a) and pore size distribution by applying the BJH method to the desorption branch of the isotherm (b).

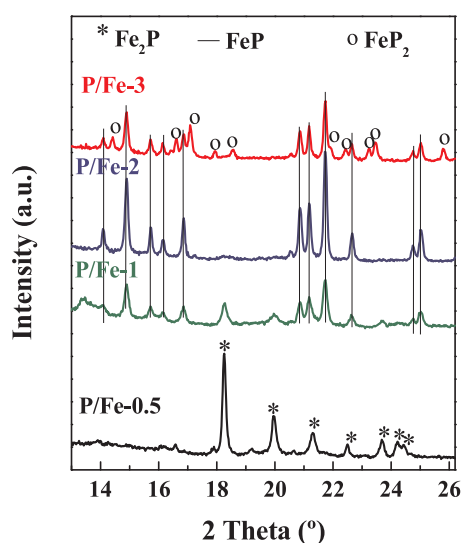


Fig. 4. X-ray diffractograms of the different samples.

Table 2

Particle size, percentage of each phase, chemisorption results and surface atomic ratios.

	Crystal phase	Size (nm)	Percentage (%) ^a	CO uptakes ($\mu\text{mol g}^{-1}$)	Dispersion (%) ^b	Surface atomic ratio	
						P/Fe	Fe/Si
P/Fe-0.5	Fe ₂ P	41.2	100	4.6	0.17	0.26	0.05
P/Fe-1	Fe ₂ P	23.6	24	12.2	0.45	0.58	0.037
	FeP	26.6	74				
P/Fe-2	FeP	42.8	100	6.6	0.25	0.73	0.044
P/Fe-3	FeP	36.5	66	4.8	0.82	0.79	0.037
	FeP ₂	52.5	34				

^a Semiquantitative analysis obtained from HighScore Plus Software from crystalline phases.

^b Calculated from CO uptakes.

1 sample than on P/Fe-0.5 one; the particle size of FeP phase follows the order: P/Fe-1 < P/Fe-3 < P/Fe-2. In general, it can be stated that samples containing different iron phosphides such is the case of P/Fe-1 and P/Fe-3 present lower particle sizes.

An estimation of the dispersion was evaluated from CO-

chemisorption measurements and the data are also included in Table 2. It has been assumed that each CO molecule is adsorbed on one active site according to previous results in literature [40]. The corresponding calculated dispersion values are low in all cases, although the values are close to those found in literature for iron phosphide [40]. From these data, it seems that FeP phase chemisorbs more CO than Fe₂P if the data corresponding to P/Fe-2 and P/Fe-0.5 are compared. Moreover, the calculated dispersion values are in accordance to XRD results, where samples with two different iron phosphide phases, P/Fe-1 and P/Fe-3, show lower particle size.

In order to get further insight of the iron phases present, Mössbauer spectroscopy was used and the corresponding spectra are lumped together in Fig. 5. In line with this, Table 3 collects the Mössbauer parameters obtained from the fit of the spectra as well as the assignment of the various spectral components to the corresponding chemical species. The spectrum recorded from the sample having a P/Fe-0.5 ratio is composed by four quadrupole doublets. The most intense ones, and accounting together for the 84% of the spectral area, correspond to the

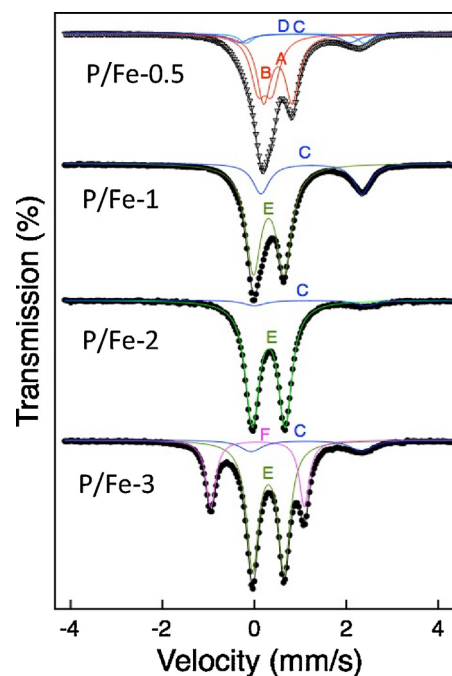


Fig. 5. Mössbauer spectra corresponding to the different phosphides.

Table 3
Mössbauer parameters obtained from the corresponding spectra fitting.

Sample	Component	δ (mm s ⁻¹)	Δ (mm s ⁻¹)	Area (%)	Assignment
P/Fe-0.5	A	0.52	0.62	46	Fe ₂ P
	B	0.23	0.30	38	
	C	1.11	2.58	7	Fe(II) phosphate
	D	0.88	2.41	9	Fe(II) phosphate
P/Fe-1.0	E	0.34	0.61	79	FeP
	C	1.14	2.40	21	Fe(II) phosphate
P/Fe-2.0	E	0.31	0.71	93	FeP
	C	1.22	2.44	7	Fe(II) phosphate
P/Fe-3.0	E	0.31	0.69	63	FeP
	F	0.07	2.04	27	FeP ₂
	C	1.13	2.40	10	Fe(II) phosphate

two crystallographic sites existing in the structure of the iron phosphide of composition Fe₂P [41]. The two minor doublets can be assigned to an Fe(II) phosphate. Both the number of Fe(II) phosphates and the range of their Mössbauer parameters is large [42], therefore, in the absence of other complementary information, it is difficult to assign the obtained parameters to a particular Fe(II) phosphate species.

The composition deduced from the spectra corresponding to the samples with P/Fe-1.0 and P/Fe-2.0 is different from that observed in the previous material. In both cases the major contribution is due to the iron phosphide of composition FeP (Table 1,[41]). The proportion of FeP is larger in the sample P/Fe = 2 (93%) than in the sample P/Fe-1.0 (79%). In both samples the minor contribution corresponds, again, to an unspecific Fe(II) phosphate. Finally, the material having P/Fe-3.0 is also dominated by the presence of FeP (63%). A contribution amount of 27% of the spectral area corresponds to the phosphorus-rich FeP₂ phosphide (Table 3,[41]). The smaller contribution, again, is due to an Fe(II) phosphate.

HRTEM micrographs for the different samples are included in Fig. 6. In the case of the samples of lower P content, it was not possible to elucidate the presence of particles. The micrographs were similar to those of iron based catalysts reported by other authors [43]. Instead, the presence of particles was more evident for P/Fe- 2 and P/Fe-3 samples, where FeP and FeP₂ phases are present. In general, Fe_xP_y particles are dispersed on the SiO₂ matrix except in some zones where a local agglomeration can be detected where the particle size cannot be calculated.

The FT-IR spectrum of the passivated sample after hydrogen activation is represented in Fig. 7a. The spectrum corresponding to FeP-0.5 sample was the only one represented in the OH-stretching region (Fig. 7a), since the other samples did not show representative contributions. It should be noted that by increasing P content the spectra became even noisier. FeP-0.5 catalyst displayed a main band located at 3747 cm⁻¹, which is attributed to the –OH stretching of isolated single silanols. The shoulder with a maximum located about 3720 cm⁻¹ is assigned to the –OH stretching of silanol group that interacts with a vicinal pair [44]. Finally, the broad and weak band located about 3700 cm⁻¹ could be attributed to the –OH stretching of surface hydroxyl groups with intermediate acid properties possibly interacting with neighboring phosphate groups, clearly noticeable for Ni₂P and CoP based samples [18].

CO molecule was used as a target molecule to determine the kind of metal sites. In all cases the spectra were carried out at low temperature (using N₂-liquid to cool the holder). This implies that the interaction between the CO molecule and the metal centers must be weak. From CO-adsorption data shown in Fig.7b, it can be observed two bands located at 2157 and 2137 cm⁻¹. The first band is attributed to the weak interaction of the CO with the –OH groups located on the surface by H-

bond, while the second band can be attributed to carbonyl species weakly coordinated over Fe-species partially reduced, possibly superimposed to some liquid-like CO [18]. In all cases, the interaction with CO is weak since both bands disappear when the temperature increases, although the P/Fe-1 sample shows stronger interactions since the band still remains after outgassing. The spectrum corresponding to P/Fe-3 sample did not show any noticeable band. The high amount of phosphorus present in this sample seems to be detrimental for IR analysis. From this figure, it can be observed that for all three samples the contribution due to OH groups is more important, and the contribution due to partially reduced iron decreases by increasing the amount of P present, indicating that CO coordination with metallic sites is favored for iron-rich phosphides.

NH₃-TPD experiments were carried out in order to assess the total acidity of the materials. Table 1 includes the total amount of ammonia desorbed for each catalyst from 100 to 500 °C and Fig. 8 the desorption profiles. The bare support desorbs a negligible amount of ammonia indicating that the observed acidity of the catalysts is mainly due to presence of the active phases. All catalysts exhibit a single desorption peak in the range of 100 to 300 °C which is associated to a weak acidic character. The total acidity increases remarkably with phosphorous content achieving its maximum value for the P/Fe = 2 catalyst.

The acidity should be related to phosphorus content present on the sample since it increases in so far as P/Fe ratio does and is expected to be associated to –OH groups as reported in literature [45,46] and also corroborated from previous IR analyses. The presence of acid sites is necessary to favor the hydrogenolysis reaction of cyclohexanol to form cyclohexene and cyclohexane [29].

The surface chemical composition of passivated catalysts was evaluated by XPS. The Si 2p and O 1s signals are centered at 103.5 eV and 532.9 eV, respectively, remaining unchanged in all catalysts. The Fe 2p core-level spectra show the coexistence of various species on the surface. The Fe 2p spectrum of the sample P/Fe = 0.5, see Fig. 9, shows the majority presence of iron(III) phosphate (711 eV) with a weak contribution owed to iron phosphide. The relative intensity of the signal corresponding to P^{δ-} rises with increasing the molar ratio P/Fe in both Fe 2p and P 2p core-level spectra. Beside this, the evolution of the Fe 2p signal shows an increase of Fe(II) as the P/Fe rises, not only for the presence of a shoulder in the region of low binding energy but also for the modification of the signal owed to the presence of a shake-up satellite. The P 2p core-level spectra of all catalysts present two contributions of the P 2p_{3/2} component centered at 133.2 eV and 128.2 eV which respectively correspond to PO₄³⁻ and P^{δ-} [30]. The phosphide species are present as Fe₂P, FeP or FeP₂ phases; and phosphate species are originated in the passivation process. Considering the surface atomic ratios compiled in Table 2, it is clearly noticeable how the phosphorus exposed on surface rises by increasing P/Fe and therefore, the iron exposed on surface is lower.

The manuscripts devoted to the use of iron in hydrotreating reactions are scarce due to the low activity of iron in these reactions. However its abundance, low toxicity and therefore its low cost make it a good candidate to face the challenges in HDO catalyst design [47]. In HDO reactions, Rezaei et al.[48] have reported that iron is an effective metal for the selective conversion of lignin-derived phenolics into aromatic hydrocarbons; when it is combined with acidic supports. Iron, an oxophilic metal, may cause repulsion to the phenolic ring, and in turn, a strong interaction with the carbonyl group, facilitating its selective hydrogenation to the corresponding alcohol [49]. The tuning among metallic and acidic sites could govern the reaction pathway followed as reported by Rezaei et al [49] when using iron catalysts supported on MCM-41 and promoted with Re and Zr to incorporate the acidic function. This bifunctional requirement is accomplished in transition metal phosphides. The use of iron phosphide in HDO reactions is scarce, as stated before, and the change in the iron-phosphorous ratio it is going to determine the stoichiometry of the iron phosphide phase formed and therefore the metallic and phosphorus surface

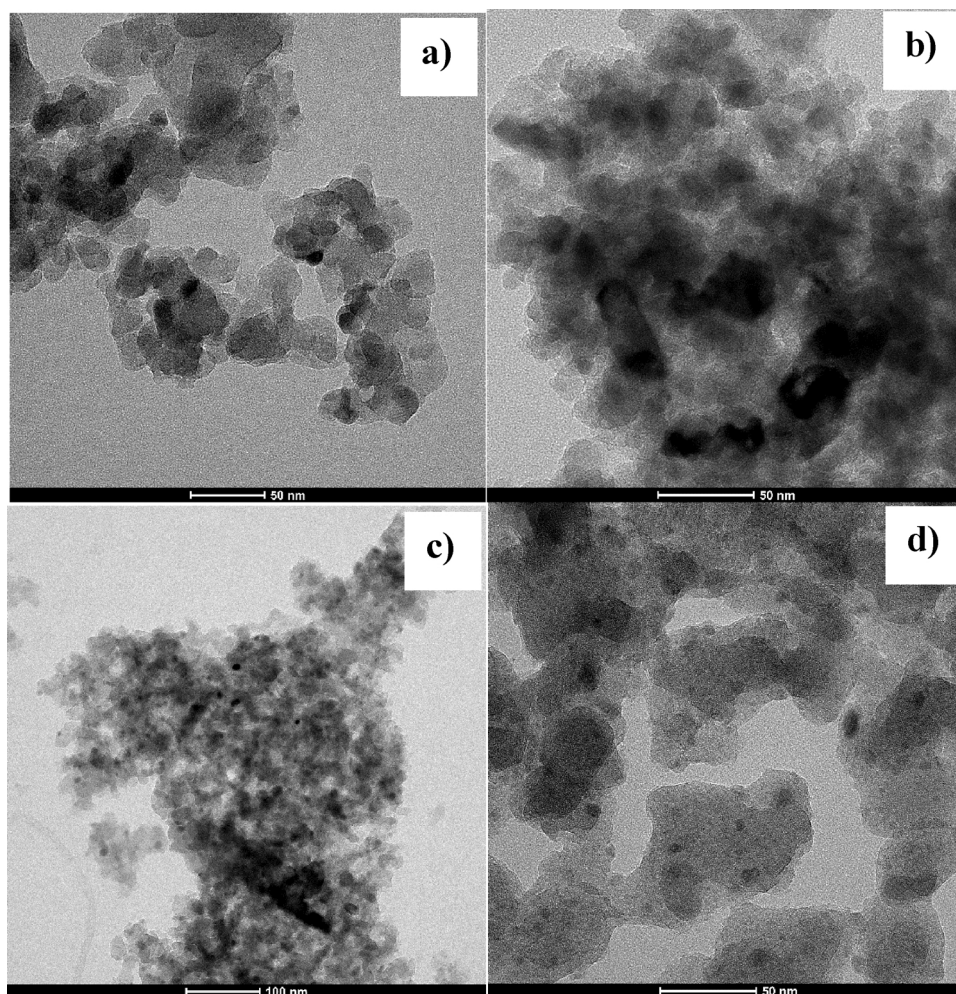


Fig. 6. HRTEM images for P/Fe-0.5, P/Fe-1, P/Fe-2 and P/Fe-3 samples.

exposure and therefore the acidity of the resultant material. From the catalytic results presented here, it seems clear that the presence of higher phosphorus content worsens the conversions results. In this sense, it has been reported for nickel and cobalt phosphide based catalysts that the incorporation of phosphorus species modifies the electronic density of the metal and diminishes the exposition of the metal sites on the surface limiting its deactivation. However, the presence of

larger amount of phosphorus can limit the amount of available active sites, which leads to poorer conversions [13,29,50]. In the present paper, by increasing the amount of phosphorus iron phosphides richer in phosphorus are formed: $\text{Fe}_2\text{P} \rightarrow \text{FeP} \rightarrow \text{FeP}_2$, iron surface exposure decreases and acidity improves. Moreover, the P/Fe molar ratio employed determines the presence of unique or mixed phases in the corresponding catalyst. All these factors determine the catalytic response

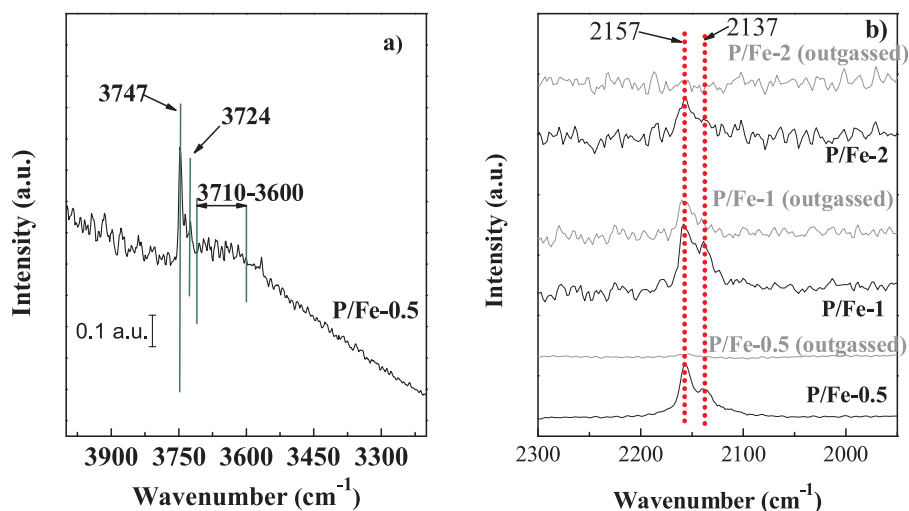


Fig. 7. FT-IR spectra in the OH-stretching region a) and after CO adsorption at $-140\text{ }^\circ\text{C}$ (black) and the same spectra with the CO outgassed at $-140\text{ }^\circ\text{C}$ (dark grey) b).

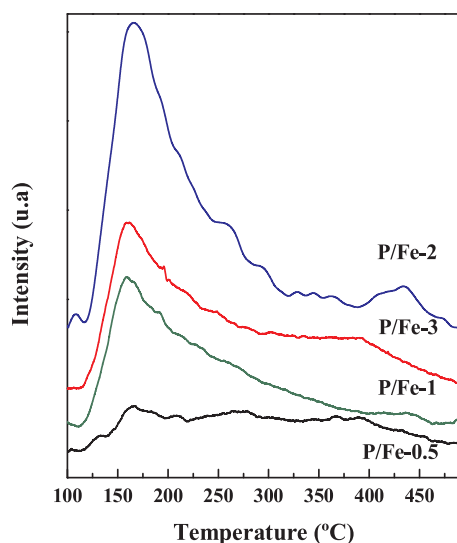


Fig. 8. Ammonia temperature programmed desorption profiles.

of the presented samples. In this regard, samples containing unique phases, such is the case of P/Fe-0.5 and P/Fe-2, presented the highest conversion values at both reaction pressures studied. If both samples are compared, Fe₂P phase is that present in P/Fe-0.5 sample and FeP that present in P/Fe-2 one. Therefore it can be concluded that Fe₂P phase is more active than FeP if conversion values are considered. Moreover, if catalytic results of all the samples are lumped together the catalytic activity of the iron phosphide phases follows the trend Fe₂P > FeP > FeP₂. In addition, if TOF values are calculated to determine the activity per active site (Table 4), the much higher activity of the P/Fe-5 sample can be highlighted compared to others at both reaction pressures studied. As previously observed from conversion values, P/Fe-0.5 and P/Fe-2 were those more active, i.e., unique phases are more appropriate to achieve better catalytic results.

TOF data can also be correlated with catalysts properties such is the case of acidity and metal surface exposure. These correlations are plotted in Fig. 10.

From this figure it is observed a relationship between iron surface exposure and TOF (Fig. 10a), thus the sample presenting the greatest iron surface exposure is that containing an iron rich phosphide, Fe₂P, and being the most active in the studied reaction, P/Fe-0.5. The better metal surface exposure was also observed from CO-IR experiments. In addition, the acidity also plays an important role in the catalytic

Table 4
Turnover frequency values.

Sample	TOF (s ⁻¹) x 10 ³	
	15 bar	5 Bar
P/Fe- 0.5	147	45
P/Fe-1	18	10
P/Fe- 2	66	29
P/Fe-3	50	21

activity of the prepared samples. Again TOF values are correlated with the catalyst acidity (Fig. 10b), the higher the better. Therefore iron phosphide stoichiometry, surface exposure of the iron and the catalyst acidity are directly correlated with the catalytic activity. These presented data are at odds with those shown for iron phosphide supported on activated carbon in the hydrodesulfurization reaction of dibenzothiophene, where FeP was more active than Fe₂P [21]. In the case, of HDO reactions the oxophilic character of iron could justify how Fe₂P phase presenting greater iron surface exposure provides more active sites to interact with oxygen from the molecules.

Taking into account the selectivity data, in spite of the change in the acidity values, all the samples follows the hydrogenation route, although the sample presenting the highest acidity, P/Fe-2, is that where the amount of benzene was noticeable, selectivity close to 15%. However, the weak nature of those sites does not favor the hydrogenolysis route, where after the first hydrogenation of the carbonyl group forming cyclohexadienols, they must be dehydrated in acidic sites to form aromatic hydrocarbons and water [51]. As suggested by other authors [52], the strength of those acidic sites are clue in order to favor the dehydration reaction to occur and to prevent catalyst deactivation. Further research is required in this regard to better understand the selectivity in HDO of iron phosphides and should be focused on the change of acidity. The presented results evidences that Fe₂P phase is the most active one in HDO.

4. Conclusions

In the present work the influence of the phosphorus content in the properties of iron-based catalysts has been evaluated as well as its activity in the phenol HDO reaction. The amount of phosphorus varied to obtain iron phosphides with different stoichiometry. When the phosphorus content was increased, it was incorporated into the iron phosphide structure and Fe₂P, FeP and FeP₂ phases were obtained, that is, iron-rich phosphide, stoichiometric iron phosphide and phosphorus-

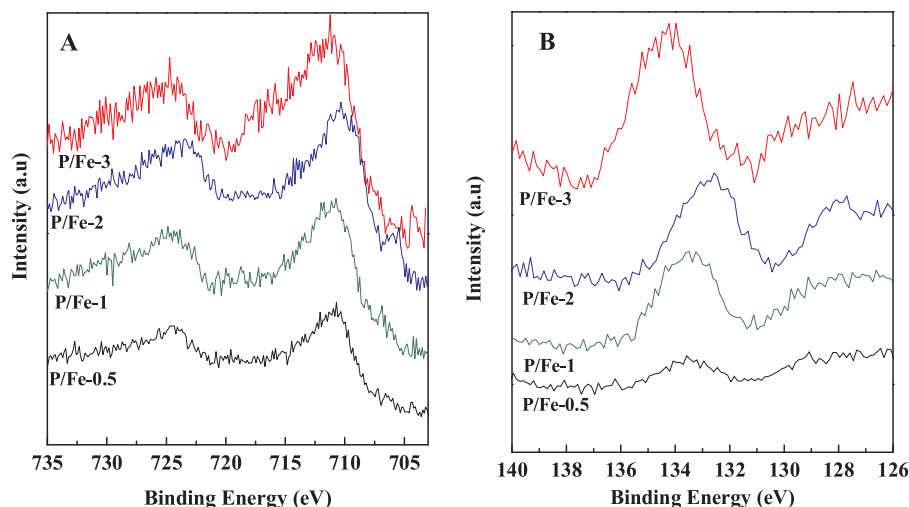


Fig. 9. Fe 2p (A) and P 2p (B) core level spectra of the studied catalysts.

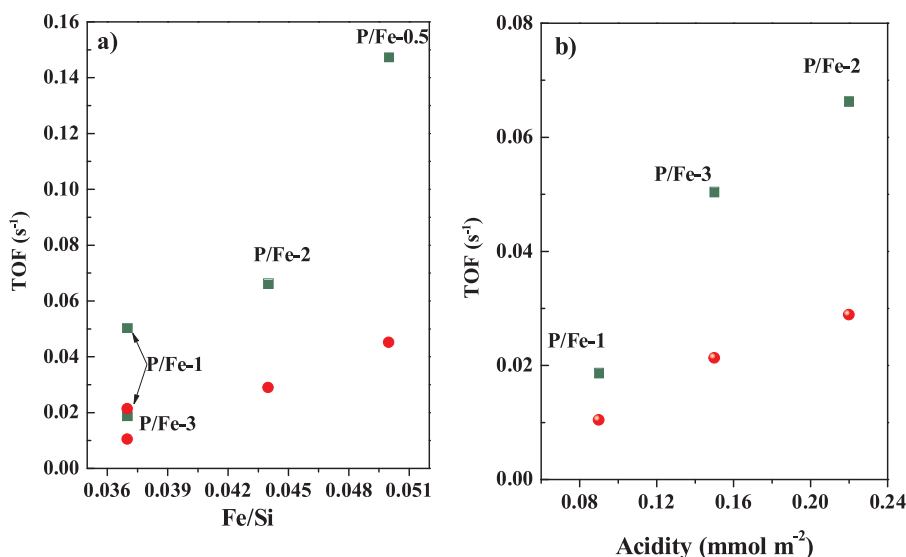


Fig. 10. Dependency of TOF with iron surface exposure and catalyst acidity. (■) 15 bar and (●) 5 bar).

rich phosphide, respectively. Furthermore, depending on the P / Fe ratio used, the catalysts synthesized contained one or two phases. The catalytic results showed that the samples were active in the HDO reaction of phenol, being those with unique phases the most active ones. In addition, the activity depended on the iron phosphide formed. Therefore, the observed trend was: Fe₂P > FeP > FeP₂. Finally, the activity per active site depended on the surface exposure of iron and the acidity of the catalyst. The results presented highlight the application of a cheap and abundant phase, such as iron in HDO reactions.

Acknowledgements

Thanks to project CTQ2015-68951-C3-3R (Ministerio de Economía y Competitividad, Spain and FEDER Funds). A.I.M. thanks the Ministry of Economy and Competitiveness for a Ramon y Cajal contract (RyC2015-17870).

References

- [1] C. Xu, R.A. Arancón, J. Labidi, R. Luque, Lignin depolymerisation strategies: towards valuable chemicals and fuels, *Chem. Soc. Rev.* 43 (2014) 7485–7500.
- [2] P.M. Mortensen, J.D. Grunwaldt, P.A. Jensen, K.G. Knudsen, A.D. Jensen, A review of catalytic upgrading of bio-oil to engine fuels, *Appl. Catal. A* 407 (2011) 1–19.
- [3] M. Patel, A. Kumar, Production of renewable diesel through the hydroprocessing of lignocellulosic biomass-derived bio-oil: a review, *Renew. Sustain. Energy Rev.* 58 (2016) 1293–1307.
- [4] S. Xiu, A. Shahbazi, Bio-oil production and upgrading research: a review, *Renew. Sustain. Energy Rev.* 16 (2012) 4406–4414.
- [5] N. Arun, R.V. Sharma, A.K. Dalai, Green diesel synthesis by hydrodeoxygenation of bio-based feedstocks: strategies for catalyst design and development, *Renew. Sustain. Energy Rev.* 48 (2015) 240–255.
- [6] T.V. Choudhary, C.B. Phillips, Renewable fuels via catalytic hydrodeoxygenation, *Appl. Catal. A* 397 (2011) 1–12.
- [7] V.K. Venkatakrisnan, W.N. Delgass, F.H. Ribeiro, R. Agrawal, Oxygen removal from intact biomass to produce liquid fuel range hydrocarbons via fast-hydro-pyrolysis and vapor-phase catalytic hydrodeoxygenation, *Green. Chem.* 17 (2015) 178–183.
- [8] H.-G. Chen, Y.H.P. Zhang, New biorefineries and sustainable agriculture: increased food, biofuels, and ecosystem security, *Renew. Sustain. Energy Rev.* 47 (2015) 117–132.
- [9] M. Toba, Y. Abe, H. Kuramochi, M. Osako, T. Mochizuki, Y. Yoshimura, Hydrodeoxygenation of waste vegetable oil over sulfide catalysts, *Catal. Today* 164 (2011) 533–537.
- [10] V.N. Bui, D. Laurenti, P. Delichère, C. Geantet, Hydrodeoxygenation of guaiacol, *Appl. Catal. B: Environ.* 101 (2011) 246–255.
- [11] S. Boullouso-Eiras, R. Lødeng, H. Bergem, M. Stöcker, L. Hannevold, E.A. Blekkan, Catalytic hydrodeoxygenation (HDO) of phenol over supported molybdenum carbide, nitride, phosphide and oxide catalysts, *Catal. Today* 223 (2014) 44–53.
- [12] P. Bui, J.A. Cecilia, S.T. Oyama, A. Takagaki, A. Infantes-Molina, H. Zhao, D. Li, E. Rodríguez-Castellón, A. Jiménez López, Studies of the synthesis of transition metal phosphides and their activity in the hydrodeoxygenation of a biofuel model compound, *J. Catal.* 294 (2012) 184–198.
- [13] X. Wang, P. Clark, S.T. Oyama, Synthesis, characterization, and hydrotreating activity of several iron group transition metal phosphides, *J. Catal.* 208 (2002) 321–331.
- [14] H.Y. Zhao, D. Li, P. Bui, S.T. Oyama, Hydrodeoxygenation of guaiacol as model compound for pyrolysis oil on transition metal phosphide hydroprocessing catalysts, *Appl. Catal. A* 391 (2011) 305–310.
- [15] J.A. Cecilia, A. Infantes-Molina, E. Rodríguez-Castellón, A. Jiménez-López, S.T. Oyama, Oxygen-removal of dibenzofuran as a model compound in biomass derived bio-oil on nickel phosphide catalysts: role of phosphorus, *Appl. Catal. B: Environ.* 136–137 (2013) 140–149.
- [16] S.T. Oyama, T. Gott, H. Zhao, Y.-K. Lee, Transition metal phosphide hydroprocessing catalysts: a review, *Catal. Today* 143 (2009) 94–107.
- [17] N. Koike, S. Hosokai, A. Takagaki, S. Nishimura, R. Kikuchi, K. Ebitani, Y. Suzuki, S.T. Oyama, Upgrading of pyrolysis bio-oil using nickel phosphide catalysts, *J. Catal.* 333 (2016) 115–126.
- [18] A. Infantes-Molina, E. Gralberg, J.A. Cecilia, E. Finocchioni, E. Rodríguez-Castellón, Nickel and cobalt phosphides as effective catalysts for oxygen removal of dibenzofuran: role of contact time, hydrogen pressure and hydrogen/feed molar ratio, *Catal. Sci. Technol.* 5 (2015) 3403–3415.
- [19] J.A. Cecilia, A. Infantes-Molina, J. Sanmartín-Donoso, E. Rodríguez-Aguado, D. Ballesteros-Plata, E. Rodríguez-Castellón, Enhanced HDO activity of Ni₂P promoted with noble metals, *Catal. Sci. Technol.* 6 (2016) 7323–7333.
- [20] X. Huang, Q. Dong, H. Huang, L. Yue, Z. Zhu, J. Dai, Facile Synthesis of Iron Phosphide Fe₂P Nanoparticle and Its Catalytic Performance in Thiophene Hydrodesulfurization, (2014).
- [21] Y. Yuan, H. Pei, H. Chen, L. Zuo, J. Shen, Preparation of Fe₂P and FeP catalysts for the hydrotreating reactions, *Catal. Commun.* 100 (2017) 202–205.
- [22] H. Du, S. Gu, R. Liu, C.M. Li, Highly active and inexpensive iron phosphide nanorods electrocatalyst towards hydrogen evolution reaction, *Int. J. Hydrogen Energy* 40 (2015) 14272–14278.
- [23] Z. Huang, C. Lv, Z. Chen, Z. Chen, F. Tian, C. Zhang, One-pot synthesis of diiron phosphide/nitrogen-doped graphene nanocomposite for effective hydrogen generation, *Nano Energy* 12 (2015) 666–674.
- [24] L. Tian, X. Yan, X. Chen, Electrochemical activity of iron phosphide nanoparticles in hydrogen evolution reaction, *ACS Catal.* 6 (2016) 5441–5448.
- [25] H. Zhao, J. Wang, Y. Dong, P. Jiang, Noble-Metal-Free iron phosphide cocatalyst loaded graphitic carbon nitride as an efficient and robust photocatalyst for hydrogen evolution under visible light irradiation, *ACS Sustain. Chem. Eng.* 5 (2017) 8053–8060.
- [26] A. Cho, J. Shin, A. Takagaki, R. Kikuchi, S.T. Oyama, Ligand and ensemble effects in bimetallic NiFe phosphide catalysts for the hydrodeoxygenation of 2-Methyltetrahydrofuran, *Top. Catal.* 55 (2012) 969–980.
- [27] H. Zhao, S.T. Oyama, H.-J. Freund, R. Włodarczyk, M. Sierka, Nature of active sites in Ni₂P hydrotreating catalysts as probed by iron substitution, *Appl. Catal. B: Environ.* 164 (2015) 204–216.
- [28] E. Rodríguez-Aguado, A. Infantes-Molina, D. Ballesteros-Plata, J.A. Cecilia, I. Barroso-Martín, E. Rodríguez-Castellón, Ni and Fe mixed phosphides catalysts for o-removal of a bio-oil model molecule from lignocellulosic biomass, *Mol. Catal.* 437 (2017) 130–139.
- [29] E. Rodríguez-Aguado, A. Infantes-Molina, J.A. Cecilia, D. Ballesteros-Plata, R. López-Olmo, E. Rodríguez-Castellón, CoxPy catalysts in HDO of phenol and dibenzofuran: effect of P content, *Top. Catal.* (2017).
- [30] J.A. Cecilia, A. Infantes-Molina, E. Rodríguez-Castellón, A. Jiménez-López, A novel method for preparing an active nickel phosphide catalyst for HDS of dibenzothio-phenone, *J. Catal.* 263 (2009) 4–15.
- [31] J.A. Cecilia, I. Jiménez-Morales, A. Infantes-Molina, E. Rodríguez-Castellón, A. Jiménez-López, Influence of the silica support on the activity of Ni and Ni₂P based catalysts in the hydrodechlorination of chlorobenzene. Study of factors

- governing catalyst deactivation, *J. Mol. Catal. A Chem.* 368-369 (2013) 78–87.
- [32] H.H. Kung, Chapter 4 surface coordinative unsaturation, *Stud. Surf. Sci. Catal.* 45 (1989) 53–71.
- [33] A. Popov, E. Kondratieva, J.-P. Gilson, L. Mariey, A. Travert, F. Maugé, IR study of the interaction of phenol with oxides and sulfided CoMo catalysts for bio-fuel hydrodeoxygenation, *Catal. Today* 172 (2011) 132–135.
- [34] D.J. Rensel, J. Kim, Y. Bonita, J.C. Hicks, Investigating the multifunctional nature of bimetallic FeMoP catalysts using dehydration and hydrogenolysis reactions, *Appl. Catal. A* 524 (2016) 85–93.
- [35] P.M. Mortensen, J.-D. Grunwaldt, P.A. Jensen, A.D. Jensen, Screening of catalysts for hydrodeoxygenation of phenol as a model compound for bio-oil, *ACS Catal.* 3 (2013) 1774–1785.
- [36] R.N. Olcese, M. Bettahar, D. Petitjean, B. Malaman, F. Giovannella, A. Dufour, Gas-phase hydrodeoxygenation of guaiacol over Fe/SiO₂ catalyst, *Appl. Catal. B: Environ.* 115-116 (2012) 63–73.
- [37] R. Olcese, M.M. Bettahar, B. Malaman, J. Ghanbaja, L. Tibavizco, D. Petitjean, A. Dufour, Gas-phase hydrodeoxygenation of guaiacol over iron-based catalysts. Effect of gases composition, iron load and supports (silica and activated carbon, *Appl. Catal. B: Environ.* 129 (2013) 528–538.
- [38] K.J. Yoon, P.L. Walker, L.N. Mulay, M.A. Vannice, Benzene hydrogenation over iron. I. Specific activities and kinetic behavior over unsupported iron and iron dispersed on SiO₂, Al₂O₃, carbon, and doped carbon, *Ind. Eng. Chem. Prod. Res. Dev.* 22 (1983) 519–526.
- [39] K.J. Yoon, M.A. Vannice, Benzene hydrogenation over iron. II. Reaction model over unsupported and supported catalysts, *J. Catal.* 82 (1983) 457–468.
- [40] M.C. Alvarez-Galvan, G. Blanco-Brieva, M. Capel-Sanchez, S. Morales-delaRosa, J.M. Campos-Martin, J.L.G. Fierro, Metal phosphide catalysts for the hydrotreatment of non-edible vegetable oils, *Catal. Today* (2017).
- [41] R. Wäppling, L. Häggström, S. Rundqvist, E. Karlsson, Mössbauer study of phosphides containing iron, *J. Solid State Chem.* 3 (1971) 276–292.
- [42] M.D. Dyar, E.R. Jawin, E. Breves, G. Marchand, M. Nelms, M.D. Lane, S.A. Mertzman, D.L. Bish, J.L. Bishop, Mössbauer parameters of iron in phosphate minerals: implications for interpretation of martian data, *Am. Mineral.* 99 (2014) 914–942.
- [43] L. Song, S. Zhang, Q. Ma, Synthesis of an iron phosphide catalyst based on sulfides and hydrodesulfurization property, *Chem. Eng. J.* 281 (2015) 281–285.
- [44] A.J.V. Roosmalen, J.C. Mol, An infrared study of the silica gel surface. 1. Dry silica gel, *J. Phys. Chem.* 82 (1978) 2748–2751.
- [45] K. Li, R. Wang, J. Chen, Hydrodeoxygenation of anisole over silica-supported Ni₂P, MoP, and NiMoP catalysts, *Energy Fuel* 25 (2011) 854–863.
- [46] Z. Pan, R. Wang, M. Li, Y. Chu, J. Chen, Deoxygenation of methyl laurate to hydrocarbons on silica-supported Ni-Mo phosphides: effect of calcination temperatures of precursor, *J. Energy Chem.* 24 (2015) 77–86.
- [47] D.A. Ruddy, J.A. Schaidle, J.R. Ferrell III, J. Wang, L. Moens, J.E. Hensley, Recent advances in heterogeneous catalysts for bio-oil upgrading via “ex situ catalytic fast pyrolysis”: catalyst development through the study of model compounds, *Green. Chem.* 16 (2014) 454–490.
- [48] P.S. Rezaei, H. Shafaghat, W.M.A.W. Daud, Aromatic hydrocarbon production by catalytic pyrolysis of palm kernel shell waste using a bifunctional Fe/HBeta catalyst: effect of lignin-derived phenolics on zeolite deactivation, *Green Chem.* 18 (2016) 1684–1693.
- [49] P. Sirous-Rezaei, J. Jae, J.-M. Ha, C.H. Ko, J.M. Kim, J.-K. Jeon, Y.-K. Park, Mild hydrodeoxygenation of phenolic lignin model compounds over a FeReOx/ZrO₂ catalyst: zirconia and rhenium oxide as efficient dehydration promoters, *Green Chem.* 20 (2018) 1472–1483.
- [50] J.A. Cecilia, A. Infantes-Molina, E. Rodriguez-Castellon, A. Jimenez-Lopez, Gas phase catalytic hydrodechlorination of chlorobenzene over cobalt phosphide catalysts with different P contents, *J. Hazard. Mater.* 260 (2013) 167–175.
- [51] X. Zhu, L.L. Lobban, R.G. Mallinson, D.E. Resasco, Bifunctional transalkylation and hydrodeoxygenation of anisole over a Pt/HBeta catalyst, *J. Catal.* 281 (2011) 21–29.
- [52] X. Zhu, L. Nie, L.L. Lobban, R.G. Mallinson, D.E. Resasco, Efficient conversion of m-Cresol to aromatics on a bifunctional Pt/HBeta catalyst, *Energy Fuel* 28 (2014) 4104–4111.